

Copyright 2012 Society of Photo-Optical Instrumentation Engineers

This paper was published in *Space Telescopes and Instrumentation 2012: Ultraviolet to Gamma Ray*, Tadayuki Takahashi, Stephen S. Murray, Jan-Willem A. den Herder, editors, Proceedings of SPIE Vol. 8443, and is made available as an electronic reprint with permission of SPIE. One print or electronic copy may be made for personal use only. Systematic or multiple reproduction, distribution to multiple locations via electronic or other means, duplication of any material in this paper for a fee or for commercial purposes, or modification of the content of the paper are prohibited.

Using the Chandra ACIS X-Ray Imager as a Background Particle Flux Detector

Peter G. Ford* and Catherine E. Grant

MIT Kavli Institute, 77 Massachusetts Avenue, Cambridge, MA, USA

ABSTRACT

The ACIS instrument aboard the Chandra Observatory can be easily damaged by low-energy charged particles, principally protons that implant themselves in the X-ray sensitive CCDs, creating charge traps that degrade the energy resolution and detection efficiency. During periods of high background radiation, ACIS must be moved out of the focal plane of the Chandra telescope and, whenever possible, this action should be taken autonomously since the spacecraft only maintains ground contact for limited periods. The EPHIN detector has been monitoring the particle background since Chandra was launched in 1999, but it is no longer sufficiently sensitive, so the question arose whether ACIS could take over this task. Examining the ACIS data archive, a particular measured quantity—the rate of occurrence of CCD pixels found to contain electric charge that exceeded a predetermined threshold—was often correlated with particle background flux. An algorithm was developed to distinguish this behavior from random fluctuations in the above-threshold rate and the algorithm parameters were adjusted to find the maximum number of high radiation flux “triggers” from the data archive with the minimum number of false positives. The algorithm has been encoded as a patch to ACIS flight software and, after extensive ground testing, has been installed within the instrument.

Keywords: Chandra, ACIS, X-ray background

1. INTRODUCTION

The ACIS X-ray imaging spectrometer¹ was launched in 1999 as part of the payload of the Chandra X-ray observatory.² After suffering significant damage to its CCDs early in the mission from low-energy charged particles,³ procedures were quickly established to put the instrument into a “radiation-protected” mode, powering down most of its electrical components and physically moving it out of the focal plane and into a shielded location at times of high background radiation.⁴ The procedures relied on the ability of particle detectors to sense the elevated fluxes, both onboard—the Electron, Proton, Helium Instrument⁵ (EPHIN)—and by explicit ground commands in response to high fluxes reported by similar monitors on other near-Earth spacecraft, *e.g.*, ACE, GOES, etc. This has worked well for many years,⁶ but higher than anticipated EPHIN temperatures have degraded its performance to such an extent that it is no longer capable of detecting radiation levels that would damage ACIS.

With EPHIN increasingly unavailable, another Chandra instrument, the High Resolution Camera (HRC) has been used as a radiation trigger since December 2008. The HRC⁷ contains an anti-coincidence shield—a plastic scintillator with photomultiplier tubes that surround the X-ray sensitive micro-channel plate array detectors. The primary purpose of this shield is to veto charged particle events that reach the detectors, but it is also capable of monitoring the radiation environment and has largely replaced EPHIN.

Past ACIS observations were examined⁸ to determine whether there was a significant correlation between ACIS data and those EPHIN energy channels that were being used to monitor the background flux that would be most damaging to ACIS. The conclusion was that about half of the EPHIN triggers coincided with rising numbers of ACIS event candidates, and suggested that the threshold crossing rate—the number of CCD pixels with values above a predetermined threshold—might be a suitable metric on which to base a trigger. Fig. 1 shows the maximum crossing rates in each 3 minute period of each ACIS observation, suggesting that many periods of high background flux have no appreciable affect on ACIS count rates. It also shows that we must be careful not

* pgf@space.mit.edu; phone +1 617 253 6485; fax 1 617 253 0861; space.mit.edu

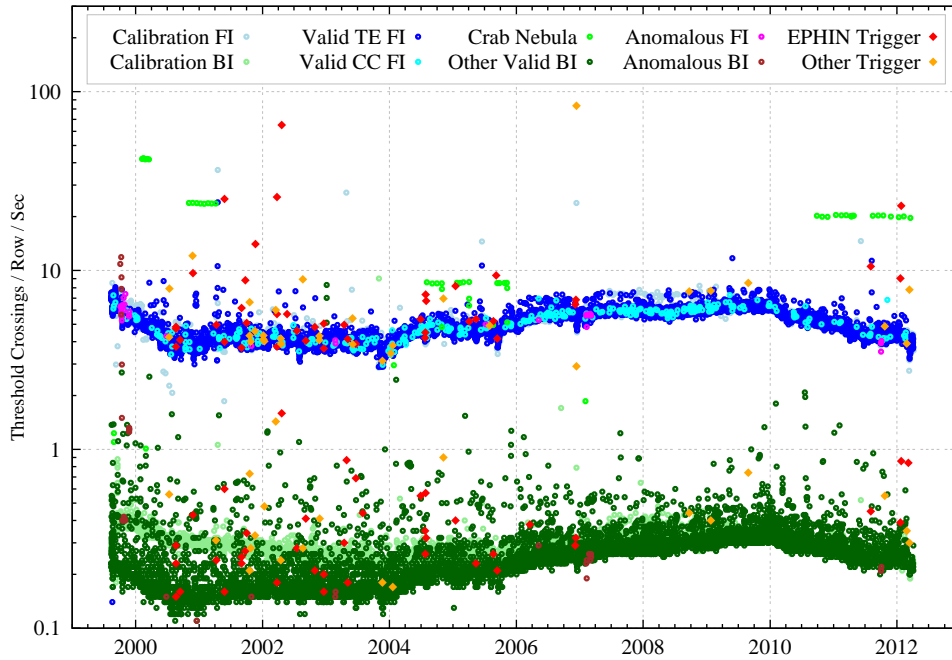


Figure 1. Maximum threshold crossing rates for all ACIS observations during 1999–2011, averaged separately over 5 minute intervals for back-illuminated (BI) and front-illuminated (FI) CCDs. Note the gradual reduction of X-ray flux in BI “calibration mode” when the CCDs were exposed to a calibration source with a half-life of ~ 3 years. Data affected by known hardware problems are marked as “Anomalous”.

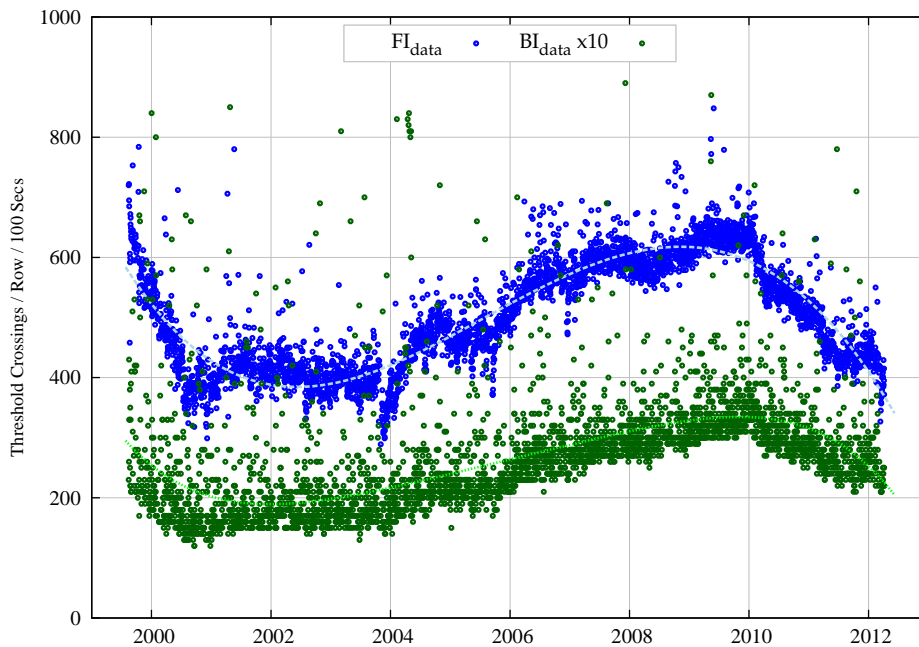


Figure 2. Polynomial fits to the threshold crossing rates for ACIS observations from October 1999 through May 2012 for front-illuminated (FI, blue) and back-illuminated (BI, green) CCDs. In the figure, BI values have been multiplied by 10 for greater visibility. Periods of high background flux and of known hardware anomalies, and observations of exceptionally bright sources, were removed before fitting. The polynomials are used to derive optimum filter parameters, as described in Section 3. The fitting process is repeated at 2-month intervals to determine whether the on-board parameters need to be updated to track changes in the average background radiation flux.

to introduce false triggers caused by bright sources, *e.g.*, the Crab nebula, or instrumental malfunctions, since, once a radiation alert is triggered, it takes ~ 24 hours for the Chandra ground support team to command the spacecraft to resume normal operations.

When the possibility was first raised of using ACIS as a radiation trigger, a problem arose—the instrument cannot move itself into its radiation shelter; only the onboard computer (OBC) can do this; but ACIS outputs its results in varying length telemetry packets that are asynchronous with respect to the spacecraft’s data formatter, making it practically impossible for the OBC to locate a trigger signal transmitted in that data stream. This leaves only one possible signal path between ACIS and the OBC—a set of 4 bilevel channels that are normally used to report the instrument’s power-up status and whether or not an observation is in progress. Happily, of the 16 possible channel values, only 14 are currently used, so one of the unused values can be assigned to a radiation trigger which can be detected by the OBC.

2. PIXEL PROCESSING

The inner working of the ACIS detector are illustrated in Fig. 3. Each active ACIS CCD sends its digitized pixel values to a Front End Processor (FEP), whose firmware locates values that are more than a pre-determined threshold above a pre-computed “bias map”. These pixels are then rescanned and those whose values exceed those of their neighbors are passed, along with the neighbors, to the Back-End Processor (BEP) for further analysis. The FEP sends the number of threshold crossings to the BEP after processing each CCD frame. The threshold levels have not changed since launch, except when observing optically-bright sources, *e.g.*, Jupiter and Venus, when the thresholds were increased to prevent the optical signal from contributing false triggers. The way the bias maps are created can also affect the threshold count. For timed-exposure runs, the bias algorithm has not changed since launch; for continuous-clocking runs, the algorithm was changed for FI CCDs in 2005, but the average threshold crossing rate was unaffected.

The BEP examines the blocks of pixel values passed by the FEPs and applies a series of filters to identify and remove events based on their CCD location, energy, and charge pattern. The purpose of these filters is to reduce the telemetry rate—from bright sources and from background events.

3. THE ALGORITHM

Since the task is to monitor the rate of background events, which the BEP is designed to filter out, it might be possible to use the rate of discarded event candidates as a trigger. In practice, however, this would be difficult to implement since the BEP would have to estimate (or be told) the number to expect, which would depend on the details of the filters and of the spatial and spectral characteristics of the source being observed. For this reason, it was decided to use the above-threshold count rates from the CCDs, ignoring any event selection or filtering.

The metric that best represents the threshold crossing rate is the number of crossings per frame, divided by the number of pixels exposed, and divided by the frame exposure time. The simplest algorithm therefore keeps one running sum of the threshold crossings and a second running sum of the frame exposure times. At fixed intervals, the first is divided by the second, yielding the average crossing rate. When these exceed a predetermined value, an alarm is posted.

The algorithm was first tested with 5 minute averages of FI and BI threshold crossing counts and with separate FI and BI count rate thresholds. The trigger criterion was that the average rate for either type must increase for n successive integration periods. The full ACIS archive of $\sim 13,000$ observations was scanned multiple times as the thresholds and n were varied. 9 genuine radiation events were found, *e.g.*, on August 4, 2011, as illustrated in Fig. 4, along with ~ 40 false triggers from several causes, as suggested by Fig. 1: known hardware anomalies, optical light leaks (*e.g.*, Jupiter), strong sources (*e.g.*, Crab), etc. The hardware anomalies were filtered out by restricting the *maximum* allowed threshold count per exposure. The strong sources were eliminated by adding a “minimum increment” criterion to the algorithm—to trigger, the n successive averages must increase by at least m per integration period.

The full parameter set is shown in Table 1. To test a given run, the rates (parameters 3 and 5) were adjusted using the polynomial fits to average crossing rates in order to compensate for their gradual change over the solar

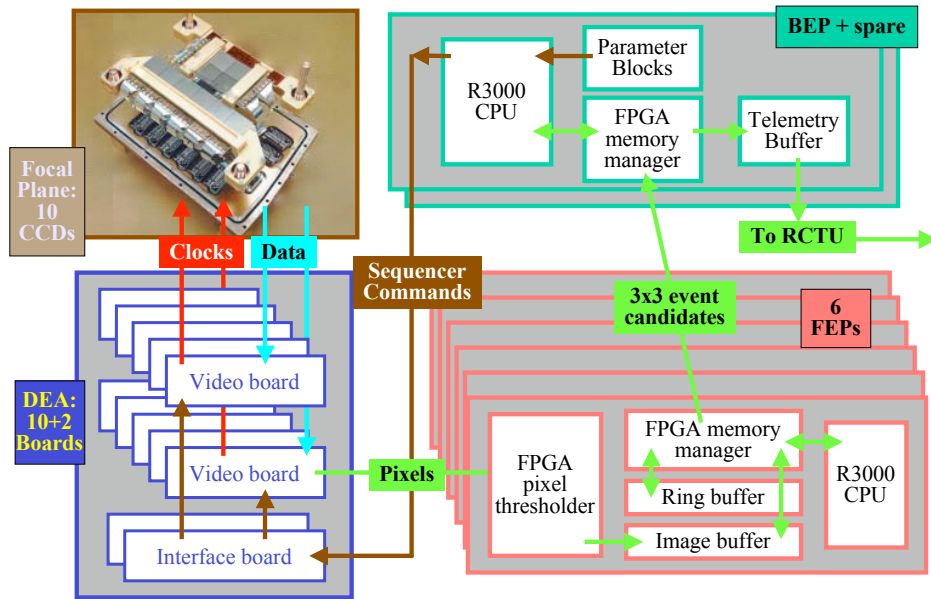


Figure 3. The ACIS instrument: X-ray sensitive CCDs (top left) send analog data to the Detector Electronics Assemblies (DEAs, bottom left), where the signals are amplified and digitized. The resulting pixel streams are passed to Front-End Processors (FEPs, bottom right) where candidate X-ray events are identified and passed to a Back-End Processor (BEP, top right). Pixel threshold levels are set by ground commands passing through the BEP CPU, under the control of a Nucleus RTX multi-tasking operating system. The BEP code has been patched to compute average threshold crossing rates from the FEPs and, when a sudden rise is found, to alert the Chandra spacecraft control computer via bilevel signal channels (not shown.)

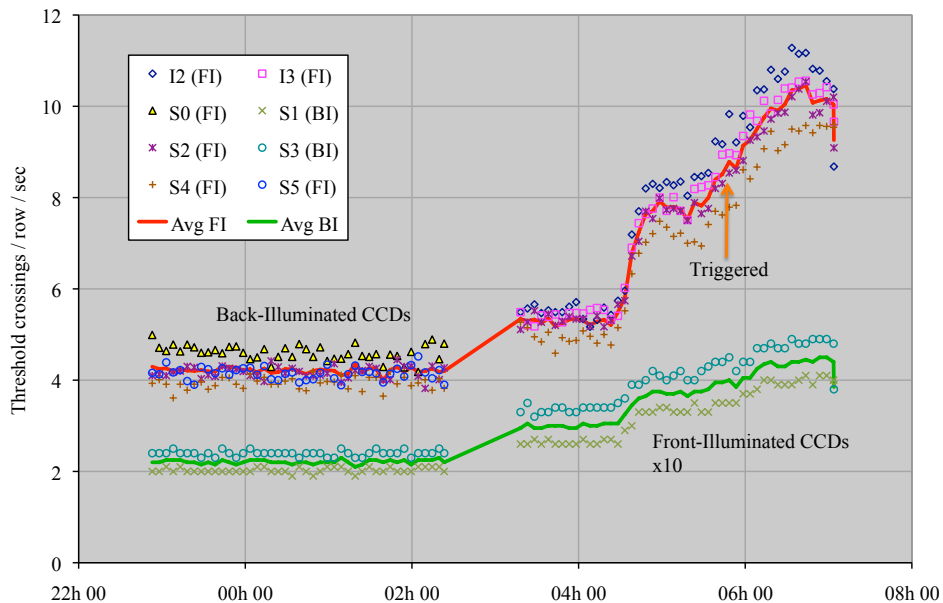


Figure 4. ACIS threshold crossing counts during a solar radiation event on August 4, 2011. The solid red and green lines represent the 5-minute averages of threshold crossing counts from front- and back-illuminated CCDs, respectively. The BI rates are multiplied by 10 for better visibility. There was no indication of an elevated count rate during the observation that ended at 02:30, but they had risen significantly by the time the next observation started at 03:10. The threshold crossing patch was not installed at that time but, had it been, it would have triggered at 05:46. In fact, the elevated background flux was detected by the HRC anti-coincidence counter⁷ and caused the OBC to put the instruments into radiation-protected mode at 07:10, at which time the ACIS threshold crossing counts were beginning to decrease.

cycle, as shown in Fig. 1. The least restrictive values of the parameters were applied to the full ACIS archive, resulting in 802 observations that triggered the algorithm. A further 66 observations were added that were known to contain intervals of high background radiation, whether or not they had any obvious effect on ACIS rates. The combined set of 868 observations was re-run through the algorithm, varying the values of each of the 6 parameters in turn, and an optimal parameter set was found that yielded the largest number of true triggers with the least number of false positives. Happily, a range of parameter values found the maximum number of true triggers—14 from November 1999 through April 2012—without any false ones, and the task became one of coding the algorithm into a sufficiently small BEP software patch.

Table 1. Parameters of the threshold crossing trigger algorithm, showing the range of values that were tested, the default values that were used from when the patch was first installed in November 2011, and the current optimal values that have been found to produce the most “good” triggers without false positives, which were installed in April 2012 and which will be updated to allow for changing background rates through the solar cycle.

	Parameter Description	Min	Max	Default ^a	Current ^b
1	Length of integration period in minutes	2	5	5	3
2	Number of successive integration periods before trigger	2	5	5	5
3	Front-illuminated (FI) count rate ^c threshold in 2000.0	670	720	700	700
4	Minimum increase in FI count rate ^c per integration	0	3	3	1
5	Back-illuminated (BI) count rate ^c threshold in 2000.0	35	55	40	45
6	Minimum increase in BI count rate ^c per integration	0	3	3	1

^a Parameter values compiled into the patch and reverted to whenever the ACIS BEP is rebooted.

^b Values uploaded in April 2012 based on extrapolations to the threshold crossing rates shown in Fig. 2.

^c Count rates are expressed as threshold crossings per 1024-pixel row per 100 seconds of CCD exposure time.

4. THE SOFTWARE PATCH

The BEP flight software was written in C++ and designed with the assistance of the Rational Rose⁹ CASE tool, in accordance with the object-oriented philosophy pioneered by G. Booch.¹⁰ This makes it particularly easy to develop patches. Although ACIS can be commanded to operate in a wide variety of modes with user-selectable exposure times, spatial windows, energy filters, etc., each type of X-ray event is described by a C++ class that inherits an *event* base class, and each exposure inherits an *exposure* base class. In the unpatched BEP code, the threshold crossing counts reported by the FEPs are extracted in a single small subroutine whose address is stored in a jump table. The patch adds a new routine that performs the same functions as the old one besides accumulating the threshold crossing count and exposure time, and updates the jump table to point to the new routine.

The number of threshold crossing pixels is transmitted from FEP to BEP for every exposure frame period, which can vary from 0.1 to 10.0 seconds, so the replacement routine intercepts the FEP-to-BEP exposure records, extracts the threshold crossing count, and accumulates the counts and exposure times, which must be examined at set intervals. The BEP CPU runs a multi-tasking operating system (Nucleus RTX) in which all threads share a common address space and are interrupted at ~100 millisecond intervals. After 640 such interrupts, a “software housekeeping” thread is activated to report the instrument status via serial telemetry, and to set the four bilevel values. This latter operation is performed by a tiny C++ routine that interfaces to the bilevel hardware registers, and, since it is called at ~64 second intervals, is an ideal candidate to be replaced by code that also tests for a high radiation condition. If the latter should occur, the routine can override the normal bilevel values, substituting the special trigger value, ‘1101’ (LED_BOOT_SPARE1).

The patch uses the 6 parameters listed in Table 1; long-term changes in the front- and back-illuminated CCD count rates must be allowed for by periodic updates from the ground. So that the parameters can be varied for specific observations, the patch actually contains three copies of the parameters: “A” for the current observation,

“B” for the next observation, and a default set, “C”. When an observation is begun, the patched code moves B to A and then moves C to B, so the parameters can be temporarily overridden for the “next” observation by updating B, or for all subsequent observations by updating B and C.

5. TESTING

In common with all changes to ACIS flight software and command parameters, the threshold crossing trigger patch was tested on a hardware simulator build from ACIS flight and engineering spares. The pixel stream was generated by a custom built signal processor that closely mimics the data sent from the video boards to the front-end processors of the flight unit. The number of over-threshold pixels was gradually increased until the patch was triggered and the bilevels were observed to change to LED_BOOT_SPARE1. Once this was found to work reliably, the patch was tested again using input from noise diodes through flight-quality video boards. Finally, it was subjected to regression testing alongside the previous flight software patches, before uplinking to Chandra and installing within ACIS on November 11, 2011. Since the OBC had not been instructed to respond to the trigger, the behavior of the patch could be monitored over the succeeding months to gain confidence that it would not generate false triggers that would have impeded Chandra operations.

Operating with its “default” parameters—the 5th column in Table 1—the patch triggered twice between November 2011 and May 2012, at times of heightened background flux on January 27 and again on May 16, and both followed within a few minutes by triggers from the anti-coincidence counter on the HRC instrument that caused the OBC to place the instruments in radiation-protected mode. As expected, the diagnostic output from the ACIS patch was written to the telemetry stream, recorded on the spacecraft, and transmitted to the ground. The values of the patch variables and accumulators precisely matched those expected from an analysis of the prior telemetry from the ACIS observations that were in process when the patches triggered.

There were a total of five high-radiation shut-downs during this same time period, so the patch failed to trigger on three occasions: on February 27 because the threshold crossing rates stayed below the limits; on March 7 because only one CCD was in use and the increased threshold crossing rate was too noisy to trigger; and on March 13 because ACIS was in the process of creating its bias maps when high HRC counts sent the instruments into radiation-protected mode. Had the current “optimal” parameters—the rightmost column in Table 1—been loaded at the time, the patch would also have triggered on February 27.

The “optimal” parameter values were loaded into the flight instrument during perigee passage on April 25 2012 and were tested by dumping patch storage areas during various stages of subsequent science runs. The values of the accumulators—of threshold crossings and exposure times—matched perfectly with those reconstructed from the transmitted telemetry. Also tested was the ability to command the patch to alter its filter parameters for the science run immediately following, after which they will revert to their “permanent” values for subsequent runs.

All tests were successful and the patch was pronounced ready to supply the Chandra on-board computer with an additional high-radiation trigger signal. Meanwhile, a companion OBC patch has been developed and tested to permit the OBC to respond to the ACIS trigger by placing the instruments into radiation-protected mode, as it does already as a result of triggers from EPIN and HRC. The patch was installed onboard on May 30 2012. Aside from periodic updates to the patch parameters as described in Section 3, ACIS is now master of its own fate.

ACKNOWLEDGMENTS

The authors wish to thank their colleagues on the ACIS instrument team, N. Adams-Wolk, M. Bautz, R. Buehler, J. Francis, K. Gage, R. Goeke, B. Lamarr, P. Plucinsky, and D. Schwartz, for their assistance and encouragement. This work was supported by NASA contracts NAS 8-37716 and NAS 8-38252.

REFERENCES

- [1] Garmire, G., Bautz, M., Ford, P., Nousek, J., and Ricker, G., “Advanced CCD Imaging Spectrometer (ACIS) instrument on the Chandra X-ray Observatory,” in [*X-Ray and Gamma-Ray Telescopes and Instruments for Astronomy*], Truemper, J. and Tanabaum, H., eds., *Proc. SPIE* **4851**, 28–44 (2003).
- [2] Weisskopf, M., Brinkman, B., Canizares, C., Garmire, G., Murray, S., and van Speybroeck, L., “An overview of the performance and scientific results from the Chandra X-ray Observatory,” *Pub. of the Astron. Society of the Pacific* **114**, 1–24 (2002).
- [3] Prigozhin, G., Kissel, S., Bautz, M., Grant, C., LaMarr, B., Foster, R., Ricker, G., and Garmire, G., “Radiation damage in the Chandra X-ray CCDs,” *Proc. SPIE* **4012**, 720 (2000).
- [4] O’Dell, S., Blackwell, W., Cameron, R., Minow, J., Morris, D., Spitzbart, B., Swartz, D., Virani, S., and Wolk, S., “Managing Radiation Degradation of CCDs on the Chandra X-ray Observatory,” *Proc. SPIE* **4851**, 77–88 (2003).
- [5] Müller-Mellin, R., Kunow, H., Fleissner, V., Pehlke, E., Rode, E., Roschmann, N., Scharmberg, C., Sierks, H., Rusznyak, P., McKenna-Lawlor, I., Sequeiros, J., Meziat, D., Sanchez, S., Medina, J., der Peral, L., Witte, M., Marsden, R., and Henrion, J., “COSTEP—Comprehensive Suprathermal and Energetic Particle Analyzer,” *Solar Phys.* **162**, 483–504 (1995).
- [6] O’Dell, S., Aldcroft, T., Blackwell, W., Bucher, S., Chappell, J., DePasquale, J., Grant, C., Juda, M., Martin, E., Minow, J., Murray, S., Plucinsky, P., Schwartz, D., Shropshire, D., Spitzbart, B., Viens, P., and Wolk, S., “Managing Radiation Reegradation of CCDs on the Chandra X-ray Observatory III,” *Proc. SPIE* **6686** (2007).
- [7] Zombeck, M., Chappell, J., Kenter, A., Moore, R., Murray, S., Fraser, G., and Serio, S., “The High resolution Camera (HRC) on the Advanced X-ray Astrophysics Facility (AXAF),” *Proc. SPIE* **2518**, 96 (1995).
- [8] Grant, C. E., LaMarr, B., Bautz, M. W., and O’Dell, S. L., “Using ACIS on the Chandra X-ray Observatory as a particle radiation monitor,” *Proc. SPIE* **7732**, 77322I (2010).
- [9] Quatrani, T., [*Visual Modeling with Rational Rose and UML*], Addison-Wesley, Boston (1997).
- [10] Booch, G., [*Object-Oriented Analysis and Design with Applications*], Benjamin/Cummings, Redwood City, CA (1994 (second edition)).